Supplemental Information

Further Information on the EQE of Planar Heterojunction OSCs with Increasing C_{60} Content

In the PHJ device architecture, increasing the C_{60} layer thickness (and thus decreasing the ClGaPc thickness) is accompanied by a broad increase in EQE from 530 nm to 730 nm. While this increase appears as a hypsochromatic shift of the 750-nm ClGaPc absorption, it is initially unclear how decreasing the ClGaPc content would result in such a drastic shift in peak absorption – such changes are not observed in the UV/Vis absorbance of neat films of ClGaPc. Instead, we look toward the increasing C_{60} layer thickness. To this end, it has been established that the Frenkel exciton bandgap in fullerenes can be quite low in energy – on the order of 1.7 eV to 2.3 eV.[39] Yang et al. showed that these low energy Frenkel excitons can be efficiently harvested when paired with a donor material at low donor concentrations.[38]

To study this effect in our devices, it is necessary to decouple the EQE contributions from ClGaPc and from C_{60}. Therefore, as a rough approach to visualize the low energy C_{60} Frenkel excitons, the 750 nm/664 nm ClGaPc peak/shoulder contributions were removed from the EQE spectra (using the ClGaPc absorption from Figure 2). Specifically, the UV/Vis absorption data was used to first identify the ClGaPc curve shape, which was normalized to the EQE values using its peak intensity. The curve was then subtracted directly from the EQE plot. The modified EQE spectra are shown in Supplemental Figure 1. These data show that the apparent shift in peak EQE is due to tail-end photocurrent contributions from C_{60} from low-energy Frenkel excitons. Consequently, the apparent shift in peak EQE is more substantial with increasing C_{60} layer thickness.

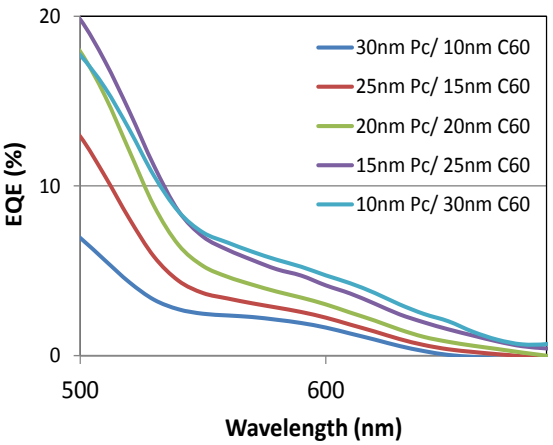

Supplemental Figure 1 - Modified external quantum efficiency spectra of the PHJ ClGaPc/C60 OSC with varying layer thicknesses. Pc contributions have been subtracted using normalized UV/Vis data.

Further Information on Negative Photocurrent Transients in donor/BHJ/acceptor OSCs

A single exponential fit was performed on the negative photocurrent transient recoveries (using a bright blue LED pulse) for the donor/BHJ/acceptor devices, as per equation (1). The τ values extracted from this analysis are shown in Supplemental Figure 2 under the label 'SE – τ, bright,' where SE refers to a single exponential fit. This negative transient recovery occurs over a much longer timescale (hundreds of μs) than the simple transient photocurrent decay observed with dim white light (tens of μs, Figure 7). This is due to the slow injection of carriers from the electrodes to compensate for the accumulated charges within the device, especially compared to the fast sweep-out of free carriers in the donor/BHJ/acceptor under dim white light where space charge effects are not as severe.

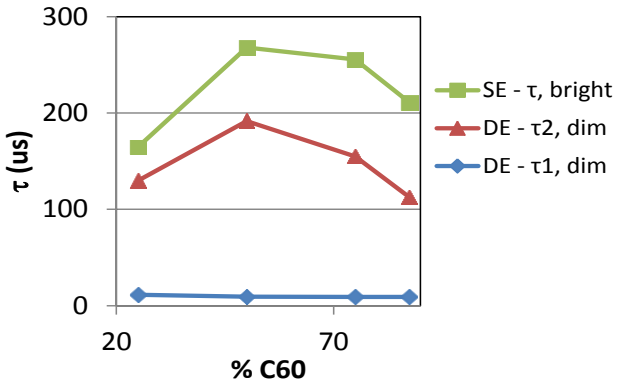

Supplemental Figure 2 – Single exponential fit (SE) and double exponential fit (DE) τ values for the transient photocurrent decays of donor/BHJ/acceptor ClGaPc:C_{60} OSCs.

We also performed a biexponential fit, as per equation (2), on the basic photocurrent transient decay curves of the same devices illuminated with a dim white LED light pulse (i.e. those curves fitted previously with a single exponential term in Figure 7).

$$I = C_1 \cdot \exp(-C_2 t) + C_3 \cdot \exp(-C_4 t), \qquad C_2 = 1/\tau_1 \; ; \; C_4 = 1/\tau_2 \tag{2}$$

In this case, the biexponential fit provides slightly better R^2 values (generally >0.999 versus >0.9), indicating that the added exponential term allows for a more accurate representation of the data. The biexponential fitted τ_1 and τ_2 values for the donor/BHJ/acceptor devices with varying mixing concentrations are also shown in Supplemental Figure 2. The fast τ_1 component of the biexponential fit is relatively constant at ~10μs for all mixing concentrations. More significantly, from Supplemental Figure 2, the slow τ_2 component of the fit is found to have the same variations with mixing concentration and a similar timing as the τ values extracted for the negative transient recovery (when illuminated with the bright blue LED pulse). It is thus strongly implied that the slow component of the biexponential fit is related to a weak space charge effect, which is present even under dim white light. One may then conclude that, even with low light intensity, the donor/BHJ/acceptor structure is susceptible to charge accumulation and associated space charge effects. These space charge effects become dominant with more intense light and, correspondingly, a higher exciton generation rate that leads to a larger number of charges within the photo-active layers. When the space charge effects become dominant and the photo-generated charges do not rapidly recombine, a negative photocurrent transient is observed.

Interestingly, while structures C and D (BHJ/acceptor and donor/BHJ respectively) did not show the negative photocurrent transients with bright red/blue LED pulses, their transient photocurrent decays were also successfully fit with a biexponential model (for dim white LED pulses). To this end, these structures' photocurrent decays showed slightly improved R^2 values with biexponential fits, had non-zero pre-exponents (C_2 and C_4 in equation (2)) and exhibited realistic τ_1 and τ_2 values (with a fast τ_1 and a slow τ_2 for each fit). However, when the biexponential fit was applied to the photocurrent decays of structures A and B (the PHJ and simple BHJ respectively), the second pre-exponential term always converged to zero, indicating that the single exponential model already adequately described the data. Having established the slow τ_2 value in the biexponential fit to be potentially related to space charge effects, it follows that structures C, D and E may all suffer from weak space charge effects. The commonality in these structures is the combination of a BHJ layer with a neat donor and/or acceptor layer, which is believed to be a contributor to these space charge effects, as discussed in the results and discussion of this manuscript.

Additional Figures (JV Characteristics)

Representative JV curves for the different architecture OSCs (with varying C_{60} content), as described in the results and discussion of the manuscript, are provided below. For the PHJ structure, C_{60} content is defined by the ratio of C_{60} layer thickness to total active layer thickness. For all other device structures, C_{60} content is defined as the amount of C_{60} within the mixed layer.

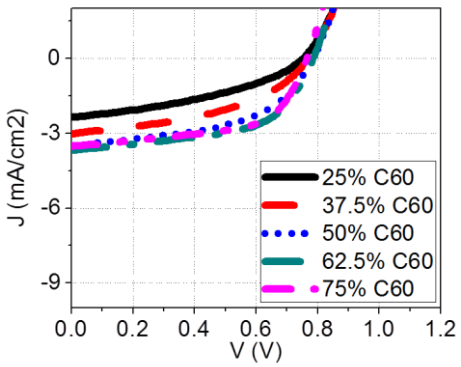

Supplemental Figure 3 – Representative JV characteristics for PHJ ClGaPc/C_{60} OSCs (structure A) with varying C_{60} content

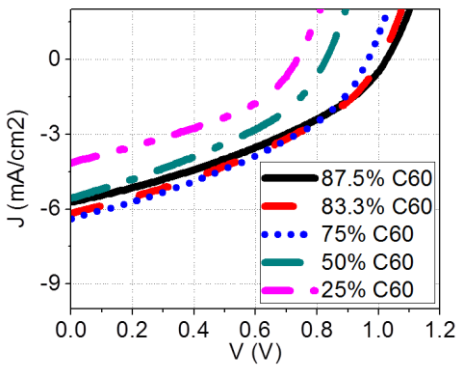

Supplemental Figure 4 – JV characteristics for BHJ ClGaPc:C_{60} OSCs (structure B) with varying C_{60} content

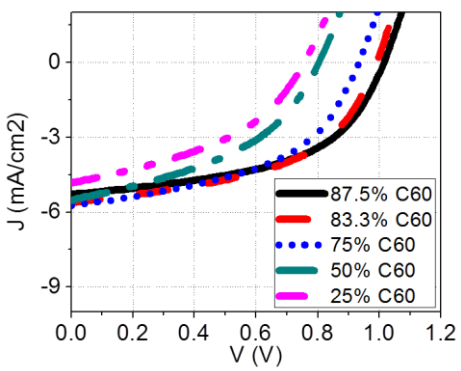

Supplemental Figure 5 – JV characteristics for BHJ/a ClGaPc:C_{60} OSCs (structure C) with varying C_{60} content

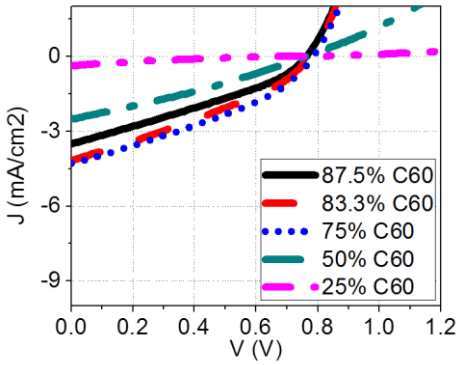

Supplemental Figure 6 – JV characteristics for d/BHJ ClGaPc:C_{60} OSCs (structure D) with varying C_{60} content

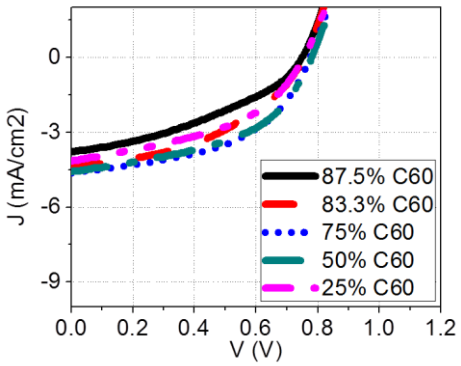

Supplemental Figure 7 – JV characteristics for d/BHJ/a ClGaPc:C_{60} OSCs (structure E) with varying C_{60} content